Optics Letters

Broadband sum-frequency generation using d_{33} in periodically poled $LiNbO_3$ thin film in the telecommunications band

Guangzhen Li,[1] Yuping Chen,[1,*] Haowei Jiang,[1] and Xianfeng Chen[1,2]

[1]State Key Laboratory of Advanced Optical Communication Systems and Networks, Department of Physics and Astronomy, Shanghai Jiao Tong University, 800 Dongchuan Road, Shanghai 200240, China
[2]e-mail: xfchen@sjtu.edu.cn
*Corresponding author: ypchen@sjtu.edu.cn

Received 18 December 2016; revised 1 February 2017; accepted 5 February 2017; posted 6 February 2017 (Doc. ID 283042); published 24 February 2017

We demonstrate the first, to the best of our knowledge, type-0 broadband sum-frequency generation (SFG) based on single-crystal periodically poled $LiNbO_3$ (PPLN) thin film. The broad bandwidth property was largely tuned from mid-infrared region to the telecommunications band by engineering the thickness of PPLN from bulk crystal to nanoscale. It provides SFG a solution with both broadband and high efficiency by using the highest nonlinear coefficient d_{33} instead of d_{31} in type-I broadband SFG or second-harmonic generation. The measured 3 dB upconversion bandwidth is about 15.5 nm for a 4 cm long single crystal at 1530 nm wavelength. It can find applications in chip-scale spectroscopy, quantum information processing, $LiNbO_3$-thin-film-based microresonator and optical nonreciprocity devices, etc. © 2017 Optical Society of America

OCIS codes: (130.3730) Lithium niobate; (310.6845) Thin film devices and applications; (190.2620) Harmonic generation and mixing; (190.4390) Nonlinear optics, integrated optics.

https://doi.org/10.1364/OL.42.000939

Broadband frequency conversion [1,2] has attracted much attention for its applications in infrared upconversion detection [3,4], wavelength division multiplexing optical networks [5], quantum key distribution [6], and especially those with ultrafast pulses such as visible ultrashort-pulse generation [7] and time-resolved spectroscopy [8,9]. Compared to second-harmonic generation (SHG), sum-frequency generation (SFG) is more promising for the abilities to mix two different fields [10,11] and to generate a spectral region that SHG cannot achieve due to the absence of efficiently fundamental lasers [12].

The main limitation of broadband SFG is the group-velocity mismatching (GVMM) [13,14], which causes the temporal walk-off effect between the fundamental-frequency (FF) and sum-frequency (SF) waves. In the spectrum domain, GVMM determines the phase-matching bandwidth of parametric process. The most direct way to broaden the bandwidth is to reduce the interaction length, but this leads to a poor trade-off between the bandwidth and the conversion efficiency. Another way is by using quasi-phase-matching (QPM) periodically domain-engineered structures [15–17]. The first broadband interaction was developed in periodically poled lithium niobate (PPLN) with type-I QPM ($o + o \rightarrow e$) by use of an off-digital nonlinear optical coefficient d_{31} (4.35 pm/V) in the telecommunications band [18]. The unique dispersion of PPLN offers a spectral range around which the dispersion nearly stands over a wide wavelength range, where one can expect the broadest upconversion bandwidth. To make use of the highest nonlinear coefficient d_{33} (27.2 pm/V), type-0 QPM ($e + e \rightarrow e$) has been developed but the bandwidth is quite narrow in the c-band [19]. Type-0 QPM also possesses the broad bandwidth property but locates it in the mid-infrared band of 2.7 μm, which limits its application in communications systems.

In addition, to meet the demand for increasing data rates in communications systems, integrated optics requires combing all the photonic components in a single chip [20,21]. Traditional waveguides, such as ridge waveguides fabricated by blade dicing, have large scattering loss due to the rough sidewall [22]; a proton exchange waveguide is low cost but with large mode size, small index contrast ($\Delta n = 0.09$), and only supports TM guiding modes [23]. Recently, an ideal platform called single-crystal $LiNbO_3$ (LN) thin film has attracted much interest for its high nonlinear and electro-optic coefficients, low intrinsic absorption loss, and large transparent windows as bulk materials have been reported [24,25]. The good confinement and strong guiding of light are due to the high-refractive-index contrast between LN and SiO_2 ($\Delta n = 0.75$). LN film has been commercially developed for photonic crystals [26], electro-optical modulators [27], and microdisk resonators [28,29]. However, as for nonlinear applications, all the demonstrated frequency conversions are SHG-based and narrow band [30–32], and no researchers have reported on the realization of SFG or broadband SFG.

In this work, we present the first, to the best of our knoledge, type-0 broadband SFG by using the highest nonlinear coefficient d_{33}, based on a z-cut 5% MgO single-crystal periodically poled lithium niobate thin film. The broad

bandwidth property was largely modulated from the mid-infrared region to the telecommunications band by engineering the thickness of PPLN from bulk crystal to nanoscale. Processed by full wafer fabrication made the sample support both TE and TM guiding modes. The unique dispersion relationship of submicrometer PPLN film supports three types of broadband SFGs in the *c*-band, including type-0. Then, we experimentally observed type-0 broadband SFG in a 700 nm thick and 20 μm period sample through the fifth-order QPM condition. The measured 3 dB upconversion bandwidth of SFG is about 15.5 nm for a 4 cm long single crystal at 1530 nm wavelength.

The PPLN thin film that we demonstrate is fabricated by direct wafer bonding, as shown in Fig. 1. Instead of starting with a single-domain $LiNbO_3$ substrate [25], a periodically poled substrate was used and processed. First, a *z*-cut 5% MgO-doped PPLN wafer with a designed domain-inversion period is implanted by He ions, as introduced in Ref. [25], forming an amorphous layer at a required depth dependent on the implantation. Another *z*-cut $LiNbO_3$ handle sample is coated by a SiO_2 layer by plasma-enhanced chemical vapor deposition and then annealed to drive off the gases trapped in the oxide layer. With a chemical mechanical polishing process, the surface roughness is reduced, enabling direct wafer bonding. The bonded pair of samples is then annealed to improve the bonding strength (16 h at 165°C + 6 h at 190°C). By a further increase in temperature (2 h at 228°C), the sample splits along the He-implanted layer. The processed thickness of the PPLN thin film can range from 200 to 1000 nm. As a slab waveguide, it maintains the excellent properties of bulk PPLN and good confinement of light. Furthermore, the structure-grating property of periodic structure can guide and confine the light in the film. Therefore, it does not need an extra waveguide structure [33,34]. Besides, the fabrication process does not damage the property of $LiNbO_3$. Therefore, it can support both TE and TM guiding modes. For the *z*-cut crystal, TE and TM waves represent the ordinary (*o*) and extraordinary (*e*) lights, respectively.

It is well known that in bulk PPLN, the SHG process usually mixes with SFG [35], and the condition of type-I broadband SFG ($o + o \rightarrow e$) has been proved to be satisfied as the same condition with broadband SHG [36–38]. Therefore, it is much easier to analyze the possibility of realizing broadband SFG together with broadband SHG. The efficient broadband upconversions in PPLN film need to satisfy three conditions:

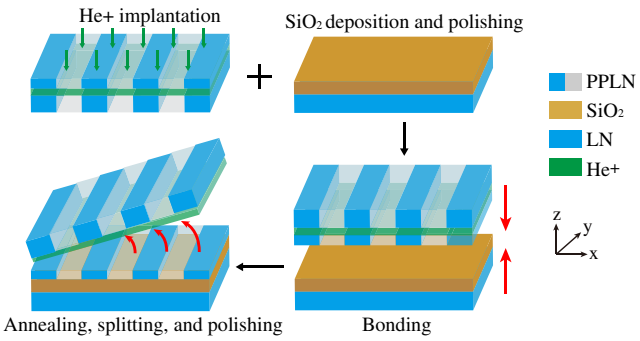

Fig. 1. Fabrication scheme of single-crystal PPLN thin film: a periodically poled $LiNbO_3$ of submicrometer thickness with designed domain-inversion period is directly bonded to a SiO_2/LN substrate.

quasi-phase matching, mode-phase matching, and group-velocity matching. For the QPM condition, it is decided by the wave-vector mismatchings (Δk), which are given by [1]

$$\Delta k_{\mathrm{SH}_i} = \frac{2\pi}{\lambda_{\mathrm{FF}_i}}\left(2n_{e/o}^{2\omega_i} - n_{e/o}^{\omega_i} - n_{e/o}^{\omega_i}\right) - \frac{2m\pi}{\Lambda}, \tag{1}$$

$$\Delta k_{\mathrm{SF}} = 2\pi\left(\frac{n_{e/o}^{\omega_1+\omega_2}}{\lambda_{\mathrm{SF}}} - \frac{n_{e/o}^{\omega_1}}{\lambda_{\mathrm{FF}_1}} - \frac{n_{e/o}^{\omega_2}}{\lambda_{\mathrm{FF}_2}}\right) - \frac{2m\pi}{\Lambda}, \tag{2}$$

where $1/\lambda_{\mathrm{SF}} = 1/\lambda_{\mathrm{FF}_1} + 1/\lambda_{\mathrm{FF}_2}$. λ_{FF_i} $(i = 1, 2)$ and λ_{SF} are the two fundamental pump wavelengths and generated SF wavelength, respectively, ω_i is the corresponding frequency, Λ is the domain-inversion period of PPLN film, and m $(\pm1, \pm3\ldots)$ is the order of QPM. $n_{e/o}^{\omega_i}$, $n_{e/o}^{2\omega_i}$, and $n_{e/o}^{\omega_1+\omega_1}$ are the refractive indices of FF, second-harmonic (SH), and SF waves calculated by Sellmeier equations [39], respectively. The subscripts *o* and *e* mean the polarization of all the involved waves can be either ordinary or extraordinary waves, respectively. For the mode-phase-matching condition, all the refractive indices in Eqs. (1) and (2) should be replaced by effective indices that can be expressed as $(n_{e/o}^{\omega})_{\mathrm{eff}} = n_{e/o}^{\omega}\sin(\theta_i)$. θ_i is the *i*th mode angle of the guiding mode decided by the dispersion relationship of the planar waveguide [40]. The overlap integrals of the interaction waves calculated are 0.34 for the 0th FF to 0th SH/SF modes and only 0.014 for the 0th to 1st modes. Therefore, we only consider the interactions between 0th to 0th modes to obtain the largest mode overlap in the following simulation.

As for the GVM condition, supposing v_{FF_i} and v_{SF} are the group velocities of FF and SF waves, respectively, the GVMM of SFG is described as $\delta_{\mathrm{SF}} = |v_{\mathrm{SF}}^{-1} - (v_{\mathrm{FF}_1}^{-1} + v_{\mathrm{FF}_2}^{-1})/2|$ [14]. It is suitable for SHG when $\lambda_{\mathrm{FF}_1} = \lambda_{\mathrm{FF}_2}$. GVMM will cause the temporal walk-off effect between the FF and SH/SF waves. The nonlinear process will be stopped if the pulses completely separate in time. GVMM can be ignored only when the crystal length is much smaller than the walk-off distance. In addition, the dependence of QPM and GVMM can be expressed as [18]

$$\frac{d(\Delta k)}{d\lambda} = \frac{4\pi c}{\lambda^2}\delta. \tag{3}$$

The GVM ($\delta = 0$) can be achieved in the spectral region where Δk takes an extremum $[d(\Delta k)/d\lambda/ = 0]$, around which the dispersion nearly stands over a wide wavelength range.

Since the PPLN film can support both TE and TM guiding modes, there exist several types of frequency conversions. First, we calculated the group velocities of different polarized FF and SH waves based on 700 nm thick PPLN film. Then, we get the GVMM for different types of SHG, as shown in Fig. 2(b). Taking $\mathrm{FF}^o + \mathrm{FF}^o \rightarrow \mathrm{SH}^e$, for example, means that two o-polarized FF waves generate an e-polarized SH wave. GVM occurs at $\delta = 0$, which exists in three types of SHG, including type-0 ($\mathrm{FF}^e + \mathrm{FF}^e \rightarrow \mathrm{SH}^e$) at 1.515 μm, which is marked as point A. Then, $\mathrm{FF}_1^e = 1.515$ μm is fixed at the central wavelength of the type-0 GVM-SHG and maintains *e*-polarization. GVMM of the three possible SFG processes is plotted in Fig. 2(a). It obviously shows that type-0 GVM-SFG ($\mathrm{FF}_1^e + \mathrm{FF}_2^e \rightarrow \mathrm{SF}^e$) occurs at the same condition with type-0 GVM-SHG at 1.515 μm, where the broadband SFG could happen. Then, we compared the wave-vector mismatchings of type-0 SFG between the 700 nm film and bulk PPLN, as shown in Figs. 2(c) and 2(d), where broadband SFG occurs

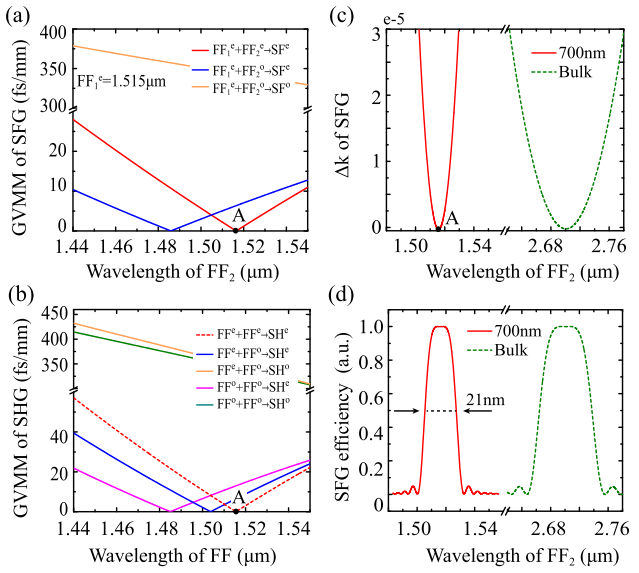

Fig. 2. Theoretical illustration of type-0 broadband SFG. GVMM for different types of (a) SFG and (b) SHG. Type-0 GVM-SFG ($\delta = 0$) (red solid line) occurs at 1.515 μm as marked point A, while $FF_1^e = 1.515$ μm is fixed at the central wavelength of type-0 GVM-SHG (red dashed line) in (b). Comparison of (c) wave-vector mismatchings and (d) SFG efficiencies of type-0 SFG between 700 nm film and bulk PPLN. Both dispersion curves take an extreme around the GVM region with designed QPM periods. The upconversion bandwidth of SFG is 21 nm for a 4 cm long thin film in the telecommunications band.

at 1.515 μm and 2.7 μm with first-order QPM periods of 4 μm and 36 μm, respectively. The 3 dB upconversion bandwidth is 21 nm for a 4 cm long thin film. The shift of the broadband SFG from 2.7 μm to 1.515 μm is caused by the variation of the refractive index of the guiding modes in the thin film, which is modulated by the planar waveguide structure [40]. The index is expressed by the effective index, $(n_e^{\omega})_{\text{eff}} = n_e^{\omega} \sin(\theta_i)$, which further affects the phase-matching conditions and leads to the shift of the center of broadband SFG. The simulation results are the same for the other two types of GVM-SFG, which confirms that broadband SFG and SHG can be simultaneously satisfied in the PPLN film and the group-velocity matching does lead to a local extreme in the dispersion curve as expressed in Eq. (3).

For the experiment, we used a 700 nm thick, 20 μm QPM domain period and 4 cm long z-cut 5% MgO PPLN film to fulfill type-0 broadband SFG, as depicted in Fig. 3. The sample is placed on a YZ-translation stage with a temperature controller at an accuracy of 0.1°C. Pump lights coming from two tunable continuous lasers (1518–1618 nm) are amplified by erbium-doped fiber amplifiers, where the polarizations are set and rotated as desired with two polarization controllers. The lights are coupled by a 50:50 fiber coupler and then inject into the nanoscale film at the front facet by a lensed fiber, which is set on a XYZ-translation stage with a resolution of 50 nm. The output lights are collected by a 20× microscope objective. The emitted FF and SF waves are separated using a dispersion lens and monitored by corresponding detectors, including power meters and optical spectrum analyzers.

Since the period we used is 20 μm, it could satisfy the fifth-order QPM ($m = 5$) type-0 broadband SFG ($\Lambda = 4$ μm for

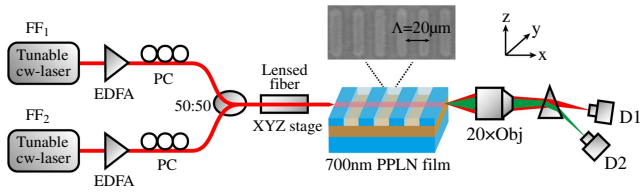

Fig. 3. Experimental setup for type-0 broadband SFG on 700 nm thickness PPLN film. EDFA, erbium-doped fiber amplifier; PC, polarization controller; 50:50, fiber coupler; D1/D2, infrared and visible detectors, including a power meter and an optical spectrum analyzer. Inset: top view of the periodically domain-engineered thin film structures.

first-order QPM) but at the cost of a large decrease in efficiency. By tuning the experimental temperature, we observed that the broadband SHG occurred at a temperature of 24.1°C and a wavelength centered at $FF_1 = 1530$ nm. The generated SHG power is 120 pW at a pump power of 60 μW (normalized efficiency of 3.3%/W). It is worth noting that the efficiency can be enhanced to 82.5%/W theoretically if using the first-order QPM period. Since the lensed fiber was not polarization maintained, we determined the excited mode of input coupled FF and the generated SH/SF waves at the output endface. The results showed that PPLN film can support both TE and TM fundamental guiding modes. However, at the largest SHG power, there was only the TM mode left. In addition, the SH wave is also in TM mode. This means that the type of broadband SHG was type-0 ($e + e \rightarrow e$), as we predicted in our former theoretical simulation. By sweeping the FF wavelength though the whole $C + L$ band, the polarizations of FF and SH maintained TM modes, which means there was no excitation of other kinds of SHG. We also measured the loss for the 4 cm long film by the Fabry–Perot interference method, which is 0.7 dB/cm.

Then, we fixed the polarizations of FF_1 and FF_2 as TM modes and observed that SF and SH modes were generated simultaneously when two pumps were located in the SHG broadband. Figures 4(a) and 4(b) show the spectra of fundamental waves of $FF_1 = 1530$ nm and $FF_2 = 1537$ nm, as well as the corresponding generated simultaneous SF and two SH waves. Under this condition, we measured the power of the generated SF wave by altering the input FF_2 wavelength while FF_1 was fixed at 1530 nm. The input powers of FF_1 and FF_2 are 30 μW and 40 μW, respectively. The SFG efficiency is plotted in Fig. 4(c), where the interaction between the two processes has been considered since they both consume energy from given pumps. The 3 dB bandwidth of SFG is 15.5 nm. In addition, we measured the SFG efficiency as a function of input FF_2 power illustrated in Fig. 4(d), while the input FF_1 power was fixed at 30 μW. The points show very good agreement with the linear fit since the conversion efficiency of SFG is proportional to the intensity of the FF_2 wave [$\eta_{\text{SF}} \propto I_{\text{FF}_1} I_{\text{FF}_2} \text{sinc}^2(\Delta k_{\text{SF}} L/2)$]. The inaccuracy of the Sellmeier equations and the idealization of the slab waveguide in the simulation cause the experimental central wavelength and bandwidth (1530 nm and 15.5 nm, respectively) shift from the theoretical values (1515 nm and 21 nm, respectively). As for the relatively low SFG efficiency, one of the main reasons is using the fifth-order QPM for the given domain period (20 μm), which can be improved by using the first-order QPM period (4 μm) PPLN substrate in the fabrication process.

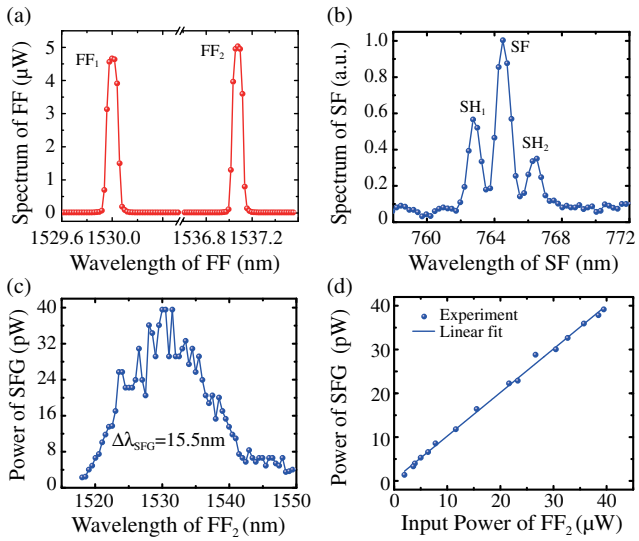

Fig. 4. Observed type-0 broadband SFG. (a) Spectra of two fundamental waves. (b) Spectra of the generated SF and two SH waves. (c) SFG power as a function of fundamental wave FF_2, while FF_1 is fixed at 1530 nm. The SFG bandwidth is 15.5 nm for a 4 cm long crystal. (d) Linear relationship between the SFG power and the input FF_2 power, while the input FF_1 power is fixed at 30 μW.

In conclusion, we demonstrated the first, to the best of our knowledge, type-0 broadband SFG based on *z*-cut 5% MgO periodically poled lithium niobate thin film. In theory, we predicted that there existed three types of broadband SFG by simultaneously satisfying the QPM and GVM conditions. We experimentally observed type-0 broadband SFG by using the highest nonlinear coefficient d_{33} on a 700 nm thick and 20 μm period sample. The measured upconversion bandwidth of SFG is 15.5 nm. The efficiency can be enhanced to 82.5%/W theoretically for the 4 cm long crystal if using the first-order QPM period PPLN substrate (4 μm) in the fabrication process and the bandwidth can be broader by shorter interaction length. This could lead to the realization of more advanced and complicated photonic integration devices and circuits that based on the broadband properties, for example, chip-scale all-optical wavelength broadcast [41], broadband spectroscopy [42], quantum information processing [43], LN-thin-film-based microresonator [44] and optical nonreciprocity devices [45], etc.

Funding. National Natural Science Foundation of China (NSFC) (11574208, 61235009).

REFERENCES

1. R. W. Boyd, *Nonlinear Optics* (Academic, 2003).
2. K. Osvay and I. N. Ross, J. Opt. Soc. Am. B **13**, 1431 (1996).
3. A. G. Lambert, P. B. Davies, and D. J. Neivandt, Appl. Spectrosc. Rev. **40**, 103 (2005).
4. D. Verreault, V. Kurz, C. Howell, and P. Koelsch, Rev. Sci. Instrum. **81**, 063111 (2010).
5. S. Arahira, H. Murai, and H. Sasaki, Opt. Express **24**, 19581 (2016).
6. N. Gisin, G. Ribordy, W. Tittel, and H. Zbinden, Rev. Mod. Phys. **74**, 145 (2002).
7. R. B. Varillas, A. Candeo, D. Viola, M. Garavelli, S. De Silvestri, G. Cerullo, and C. Manzoni, Opt. Lett. **39**, 3849 (2014).
8. O. Kuzucu, F. N. Wong, S. Kurimura, and S. Tovstonog, Opt. Lett. **33**, 2257 (2008).
9. L. Foglia, M. Wolf, and J. Stähler, Appl. Phys. Lett. **109**, 202106 (2016).
10. A. J. Lee, H. M. Pask, and T. Omatsu, Appl. Phys. B **122**, 1 (2016).
11. J. S. Dam, P. Tidemand-Lichtenberg, and C. Pedersen, Nat. Photonics **6**, 788 (2012).
12. Y. Lü, X. Zhang, X. Fu, J. Xia, T. Zheng, and J. Chen, Laser Phys. Lett. **7**, 634 (2010).
13. A. Weiner, IEEE J. Quantum Electron. **19**, 1276 (1983).
14. C. Rulliere, *Femtosecond Laser Pulses* (Springer, 2005).
15. J. Armstrong, N. Bloembergen, J. Ducuing, and P. Pershan, Phys. Rev. **127**, 1918 (1962).
16. H. S. Chan, Z. M. Hsieh, W. H. Liang, A. Kung, C. K. Lee, C. J. Lai, R. P. Pan, and L. H. Peng, Science **331**, 1165 (2011).
17. M. Ahlawat, A. Bostani, A. Tehranchi, and R. Kashyap, Opt. Lett. **38**, 2760 (2013).
18. N. E. Yu, J. H. Ro, M. Cha, S. Kurimura, and T. Taira, Opt. Lett. **27**, 1046 (2002).
19. G. Z. Li, Y. P. Chen, H. W. Jiang, and X. F. Chen, Photon. Res. **3**, 168 (2015).
20. H. Leng, X. Yu, Y. Gong, P. Xu, Z. Xie, H. Jin, C. Zhang, and S. Zhu, Nat. Commun. **2**, 429 (2011).
21. H. Jin, F. Liu, P. Xu, J. Xia, M. Zhong, Y. Yuan, J. Zhou, Y. Gong, W. Wang, and S. Zhu, Phys. Rev. Lett. **113**, 103601 (2014).
22. T. W. Neely, L. Nugent-Glandorf, F. Adler, and S. A. Diddams, Opt. Lett. **37**, 4332 (2012).
23. J. Sun and C. Xu, Opt. Lett. **37**, 2028 (2012).
24. M. M. Fejer, G. Magel, D. H. Jundt, and R. L. Byer, IEEE J. Quantum Electron. **28**, 2631 (1992).
25. G. Poberaj, H. Hu, W. Sohler, and P. Guenter, Laser Photon. Rev. **6**, 488 (2012).
26. L. Cai, H. Han, S. Zhang, H. Hu, and K. Wang, Opt. Lett. **39**, 2094 (2014).
27. H. C. Huang, J. I. Dadap, G. Malladi, I. Kymissis, H. Bakhru, and R. M. Osgood, Opt. Express **22**, 19653 (2014).
28. C. Wang, M. J. Burek, Z. Lin, H. A. Atikian, V. Venkataraman, I. C. Huang, P. Stark, and M. Lončar, Opt. Express **22**, 30924 (2014).
29. J. Lin, Y. Xu, Z. Fang, M. Wang, J. Song, N. Wang, L. Qiao, W. Fang, and Y. Cheng, Sci. Rep. **5**, 8072 (2015).
30. R. Geiss, S. Saravi, A. Sergeyev, S. Diziain, F. Setzpfandt, F. Schrempel, R. Grange, E.-B. Kley, A. Tünnermann, and T. Pertsch, Opt. Lett. **40**, 2715 (2015).
31. L. Chang, Y. Li, N. Volet, L. Wang, J. Peters, and J. E. Bowers, Optica **3**, 531 (2016).
32. A. Rao, M. Malinowski, A. Honardoost, J. R. Talukder, R. Rabiei, P. Delfyett, and S. Fathpour, "Second-harmonic generation in periodically-poled thin film lithium niobate wafer-bonded on silicon," arXiv:1609.09117 (2016).
33. S. Kim and V. Gopalan, Mater. Sci. Eng. B **120**, 91 (2005).
34. F. Van Laere, G. Roelkens, M. Ayre, J. Schrauwen, D. Taillaert, D. Van Thourhout, T. F. Krauss, and R. Baets, J. Lightwave Technol. **25**, 151 (2007).
35. L. Golovan, G. Petrov, V. Y. Gayvoronsky, I. Pritula, and V. Yakovlev, Laser Phys. Lett. **11**, 075901 (2014).
36. M. Gong, Y. Chen, F. Lu, and X. Chen, Opt. Lett. **35**, 2672 (2010).
37. J. Zhang, Y. Chen, F. Lu, and X. Chen, Opt. Lett. **16**, 6957 (2008).
38. W. Dang, Y. Chen, M. Gong, and X. Chen, Appl. Phys. B **110**, 477 (2013).
39. O. Gayer, Z. Sacks, E. Galun, and A. Arie, Appl. Phys. B **91**, 343 (2008).
40. A. W. Snyder and J. Love, *Optical Waveguide Theory* (Springer, 2012).
41. M. Ahlawat, A. Tehranchi, K. Pandiyan, M. Cha, and R. Kashyap, Opt. Express **20**, 27425 (2012).
42. K. Huang, X. Gu, H. Pan, E. Wu, and H. Zeng, Appl. Phys. Lett. **100**, 151102 (2012).
43. S. Tanzilli, W. Tittel, M. Halder, O. Alibart, P. Baldi, N. Gisin, and H. Zbinden, Nature **437**, 116 (2005).
44. W. C. Jiang and Q. Lin, Sci. Rep. **6**, 36920 (2016).
45. L. Chang, X. Jiang, S. Hua, C. Yang, J. Wen, L. Jiang, G. Li, G. Wang, and M. Xiao, Nat. Photonics **8**, 524 (2014).